Engineering Geological and Petrological Characterization of Paleoweathered Rock in The K1/j2 Contact Zone in the Ordos Basin, China

Tingen Zhu
China University of Mining and Technology - Xuzhou Campus: China University of Mining and Technology
wenping Li (wpligroup@cumt.edu.cn)
China University of Mining and Technology
Qiqing Wang
China University of Mining and Technology - Xuzhou Campus: China University of Mining and Technology
Yanbo Hu
China University of Mining and Technology - Xuzhou Campus: China University of Mining and Technology

Research Article

Keywords: paleoweathered rock, point load strength, uniaxial compressive strength, engineering geological characteristics

Posted Date: March 9th, 2021

DOI: https://doi.org/10.21203/rs.3.rs-217978/v1

Version of Record: A version of this preprint was published at Environmental Earth Sciences on March 1st, 2022. See the published version at https://doi.org/10.1007/s12665-022-10293-0.

Engineering geological and petrological characterization of paleoweathered rock in the K_1/J_2 contact zone in the Ordos Basin, China

Tingen Zhu[1] • Wenping Li[1] • Qiqing Wang[1] • Yanbo Hu[2]

Correspondent author: Wenping Li, wpligroup@cumt.edu.cn

[1] School of Resources and Geosciences, China University of Mining and Technology, Xuzhou 221116, Jiangsu, China

[2] School of Transportation Engineering, Nanjing University of Technology, Nanjing 210009, Jiangsu, China

Abstract

Various geological processes (mineral composition, structure, tectonics and weathering, etc.) affect the physical-mechanical properties of rock. Petrological and engineering geological characteristics of paleoweathered rock (PWR) from the K_1/J_2 contact zone are described in detail via field investigation and experimental testing. This PWR exhibits mainly sandy grains and mud structures, layered and massive strata, and calcareous and argillaceous cements; fissures are developed and often filled with argillaceous and detrital materials; 9 minerals and 7 oxides are present, and quartz is present in each sample. Long-term weathering results in a consistent bulk density and high porosity due to the transformation of primary minerals into secondary clay minerals, forming PWR that undergoes argillization in water. The axial point load strength (PLS) is the largest among the tested PLSs, followed by the diametral PLS, and the irregular PLS. The uniaxial compressive strength (UCS) varies widely, but the results are reliable. The mineralogical, physical and mechanical properties of the PWR are compared to predict one parameter from another and study their mutual influence. The PLS and UCS of the PWR are negatively correlated with the elastic mineral group (EMG) content, weathering alteration indexes, water content, and total porosity and positively correlated with the quartz content, brittle mineral group (BMG) content, bulk density, real density, and longitudinal wave velocity. The UCS and the PLS, axial (diametral) PLS and irregular PLS are positively correlated. These results provide a theoretical basis for physical and mechanical property prediction of PWR masses and rapid estimation of UCS in engineering.

Keywords: paleoweathered rock, point load strength, uniaxial compressive strength, engineering geological characteristics

1. Introduction

The behavior of rock under stress is studied in engineering geological research, and the quantification of engineering geological and petrological characteristics is very useful in the interpretation of rock behavior. Rock properties are actually affected by various geological processes, such as mineral composition and content, structure, tectonics and weathering (Pappalardo et al. 2016). Therefore, in geological scenarios characterized by complex geological dynamic evolution, it is very meaningful to describe the engineering geology and petrological characteristics in detail.

The inspiration of this study is the occurrence of water (mud) inrush accidents caused by coal mining in the Ordos Basin (Guo et al. 2020; Lu et al. 2018). In recent years, large-scale coal mining in some mines in the Ordos Basin has caused the deformation (failure) of overlying strata, a decline in impermeable capacity, the leakage of Cretaceous water bodies, water (mud) inrush accidents, and damage to the ecological environment (zhu et al. 2020). Through our statistical analysis of borehole data in the mining area of the Ordos Basin and a large number of field geological surveys, we found that PWR in the K_1/J_2 contact zone generally exists in the central part of the Ordos Basin, serving as

the key aquifuge directly below the Cretaceous water body, and that the deformation and failure of PWR is the root cause of the abovementioned series of problems.

Some physical and mechanical properties of rock depend on geological characteristics, which causes the rock to show inhomogeneity, discontinuity and anisotropy (Douma et al. 2017; Vikram et al. 2012). There are many studies on the geological characteristics of rocks worldwide, mainly focusing on petrography, petrochemistry, structure, physical mechanics, hydrogeology and other characteristics (Zhang et al. 2013; Ulyasheva et al. 2016; Marques et al. 2017; Menningen et al. 2018; Vonto et al. 2020; Bai et al. 2020). Many scholars have been searching for potential relationships between certain geological characteristics and rock mechanical properties (Chatterjee et al. 2002; Tamrakar et al. 2007; Sousa et al. 2005). For example, the mineral composition and contents, density, porosity, water content and wave speed of rock will affect its mechanical properties and lead to the anisotropy of the rock (Meng et al. 2007; Cantisani et al. 2013; Undul et al. 2016; Fereidooni 2016; Sun et al. 2017; Wang et al. 2019). Many scholars have carried a considerable amount of research on the relationship between rock PLS and UCS (D'Andrea et al. 1965; Broch et al. 1972; Gunsallus et al. 1984; Hawkins 1998; Kahraman 2001; Quane 2003; Palchik et al. 2004; Sabatakakis et al. 2008; Basu et al. 2010; Heidari et al. 2012; Xiang 1981; Wei 1982; Li et al. 2013; Wong et al. 2017; Liu et al. 2019). The above studies have improved the understanding of the macro- and microproperties of rocks. However, there are no reports on related studies of PWR of the K_1/J_2 contact zone of the Ordos Basin.

Therefore, in this work, PWR samples were collected from the K_1/J_2 contact zone in the Ordos Basin to test the mineral composition and contents, chemical element composition and contents, water content, density, porosity, longitudinal wave velocity, expansion rate, PLS and UCS of the PWR. The aim is to study the petrological and engineering geological characteristics of the PWR in the K_1/J_2 contact zone. Through the regression analysis method, the relationship between each feature data type and the degree of influence of each feature data type on the engineering characteristics of PWR are studied. The results of this research provide a theoretical basis for the physical-mechanical properties of PWR masses and the generalization of geological models in the next step of research and are of great significance to the safety of coal mining and ecological environment protection in the Ordos Basin.

2. Geological setting and sampling site

The Ordos Basin is a multicycle superimposed basin developed on the North China Craton and currently located in the western North China Craton (Xu et al. 2013). In the middle of the Yanshan tectonic movement, during the Late Jurassic to Early Cretaceous, the Ordos Basin developed considerable thrust nappe structures, forming a basin pattern of uplift in the east and subsidence in the west, resulting in the Jurassic Anding Formation and the overlying Cretaceous Zhidan Group (Luohe Formation) being in unconformable contact (Zhang et al. 2007; Jia et al. 2005). The Upper Jurassic strata were intermittently deposited for approximately 20 million years (Huang 2019), and PWR is preserved on the top of the Jurassic Anding Formation. According to the drilling data of the Yingpanhao mining area, PWR is widely present at the K_1/J_2 contact zone, in Shenmu County (①), Jingbian County (②), the Ansai district of Yan'an city (③), and Ganquan County (④) (Fig. 1a). All outcrops of PWR are found in the K_1/J_2 contact zone (Fig. 1b). The investigation shows that the PWR is characterized by purple-red to gray coloring and is generally paleoweathered sandstone, sandy mudstone and mudstone. These sedimentary characteristics consistently indicate the arid and hot sedimentary climate in the area. This is consistent with the characteristics of the arid climate reflected

by the sporopollen, the specialized combination of Psilunio, and the ostracod Timiriasevia-Darwinula genera found in the research area (Wang 2011).

In this work, the PWR samples of the K_1/J_2 contact zone were collected from core drilling in the Yingpanhao mining area and field geological survey sampling. The 17 groups of samples are from five regions. Each group of PWR samples was tested to determine the mineral composition, chemical element composition, density, porosity, water content, longitudinal wave velocity, expansion rate, PLS and UCS. Notably, the diametral and axial loading PLS test specimen diameter was nearly 50 mm, and the lengths were nearly 30 mm and 70 mm, respectively; the size of the test pieces for the irregular lump testing met the following requirements: the shortest side length was 30-80 mm, the ratio of the distance between the loading points (D) to the average width of the smallest load surface passing through the two loading points (W) was 0.5-1.0, and the distance from the loading point to the free end (L) was greater than 0.5D. The UCS sample diameter and length dimensions were approximately 50 mm and 100 mm, respectively. A total of 342 PWR samples were prepared for strength testing, but only 216 valid samples were recorded, including 19 samples for the UCS testing (2 failed), 19 samples for the diametral testing (2 invalid), 18 samples for the axial testing (1 invalid) and 286 samples for the irregular lump testing (31 invalid).

3 Petrological features

This section describes how field geological surveys, scanning electron microscopy (SEM), X-ray diffraction (XRD) and X-ray fluorescence (XRF) methods were used to qualitatively characterize the macroscopic structure and microscopic mineral structure, quantitatively analyze the mineral composition and chemical element composition, and more intuitively understand the mineralogy and petrology characteristics of the PWR.

3.1 Methodology

3.1.1 SEM

The scanning electron microscope model used in this work is an FEI Quanta TM 250; microstructure and composition characterization images of PWR samples were collected. The main performance indicators of the instrument are as follows: high-vacuum mode resolutions: ⩽ cu nm at 30 kV (SE), ⩽4.0 nm at 30 kV (BSE), and ⩽and nm at 3 kV (SE); magnification range: 6-100 million times; and acceleration voltage : 0.2-30 kV.

3.1.2 XRD

The X-ray diffractometer model used in this work to perform diffraction analysis of the PWR samples is an X-Ray Diffraction from D8 Advance. The main performance indicators of this instrument were as follows: measurement accuracy: angle reproducibility of ±0.0001°; radius of the goniometer: ⩾0.0 mm; diameter of the angle measuring circle continuously changed; minimum step length: 0.0001°; angle range (2θ): -110~168°; temperature range: 20~1200urengle range (2θ 3 kW; stability ±0.01%; and tube voltage 20~60 kV (1 kV/1 step). Semiquantitative mineralogical analysis of PWR diffraction data was performed using MDI Jade6 diffraction analysis software. The determination of the mineral phase in each sample was achieved by comparison with the standard spectrum of various mineral phases. The semiquantitative analysis of minerals was performed with MDI Jade6 software according to the steps of background deduction, smoothing, peak search and calculation; for each sample, the contents of various minerals were calculated by the K value method, and the relevant values were provided by the PDF card in MDI Jade6 software (Zhao et al. 2019). The semiquantitative K value method is as follows: suppose the mixture contains two phases, No. 1 and No. 2, and the characteristic peak intensities of 100% of their relative intensities are measured as I1

and I2; check the standard card library to determine their K values ($K = I/I_{\alpha}$—Al_2O_3), which are K_1 and K_2, respectively; then, $1\% = \frac{\frac{I_1}{K_1}}{\frac{I_1}{K_1}+\frac{I_2}{K_2}} \times 100\%$, and $2\% = \frac{\frac{I_2}{K_2}}{\frac{I_1}{K_1}+\frac{I_2}{K_2}} \times 100\%$.

3.1.3 XRF

The XRF spectrometer model used in this paper is an X-Ray Fluorite Spectroscopy S8 Tiger and was used to analyze the main and trace element types and contents of the PWR samples. The main performance indicators of the instrument are as follows: scanning method: sequential scanning; hardware indicators: power 4 kW, maximum voltage: 60 kV; maximum current: 170 Ma; element detection range: Be(4)-U(92); and detection limit: PPM-100%. In recent years, the chemical index of alteration (CIA), chemical index of weathering (CIW) and plagioclase index of alteration (PIA) have been widely used to reflect the source area degree of weathering (Shaldybin et al. 2019; Elena et al. 2015; Farkas et al. 2018) and are defined as follows: CIA=[Al_2O_3/(Al_2O_3+CaO+Na_2O+K_2O)]×100, CIW=[Al_2O_3/(Al_2O_3+CaO+Na_2O)]×100, PIA=[Al_2O_3-K_2O/(Al_2O_3+CaO+Na_2O-K_2O)].

3.2 Petrological characterization

Through numerous surveys of PWR outcrops in the K_1/J_2 contact zone, a preliminary understanding of the macrostructure characteristics of PWR has been obtained. The color of PWR is mainly light red to purple-red, light gray to gray, and light green. The structure is dominated by gravel, fine grains, silt grains and pelites, and a few are cryptocrystalline (Fig. 2 e-f). The tectonic activity mainly formed layered and massive strata, a few of which are earthy (Fig. 2 a-d). The cements are mainly calcareous and argillaceous, with sparse iron cements (Fig. 2 a-c). Joints and fractures are developed, often filled with mud and clastic material.

The XRD semiquantitative analysis results are shown in Fig. 3, reflecting the mineral composition of PWR in the K_1/J_2 contact zone in the Ordos Basin. Clearly, all the PWR collected from outcrop sections contains quartz. This is because quartz is the most stable mineral among the detected mineral types; quartz is also one of the most stable minerals on Earth's surface (Sun et al 2013). The remaining detected minerals (calcite, dolomite, albite, muscovite, kaolinite, illite, montmorillonite, and chlorite) vary depending on the sampling location. For example, the calcite of the AS-1 and GQ-2 groups has been weathered and decomposed into other secondary minerals, and the calcite and dolomite of the SM-1 and SM-2 groups have been weathered into other secondary minerals. The rock-forming minerals listed above were identified and described according to the "Geotechnical Investigation and Design Manual" (Lin et al 1996) and SEM images. Quartz is kidney-shaped or irregular (Fig. 2 j), hard and brittle, and has strong resistance to weathering. Calcite often forms crystal clusters and granular or nodular shapes (Fig. 2 k) and is brittle. Dolomite is often granular or massive (Fig. 2 l) and brittle, with curved surfaces and stripes. Feldspar is often platy or columnar (Fig. 2 m) and brittle, with stripes visible on the cleavage surface. Muscovite is flaky or scaly, stacked and elastic. Kaolinite is generally lumpy, flaky, or earthy, with a slippery feel, easily absorbs water, and has a plastic viscosity when wet. Illite is generally earthy, with a greasy feel, and is weaker than muscovite. Montmorillonite is often earthy or cryptocrystalline, with a slippery feel, and swells significantly after being immersed in water. Chlorite is scaly, has a slippery feel, is flexible, and has poor elasticity.

XRF was used to analyze the main elemental composition of the PWR samples, and the results are shown in Fig. 4. The PWR mainly contains 7 kinds of oxides; on the outcrop profile, SiO_2 is the oxide with the largest proportion in most sample groups. Notably, the outcrop sections contain a large

amount of Fe_2O_3, but XRD analysis of some samples corresponding to these groups (JB-1 to JB-5, JB-7, AS-1, GQ-1, GQ-2) did not detect chlorite, which may have been decomposed into amorphous iron. In Fig. 4, the changes in CIA, CIW and PIA of PWR are also shown. High CIA and CIW values reflect relatively strong weathering in warm and humid climates; conversely, low CIA values reflect relatively weak weathering in cold and dry climates. PIA is suitable for judging the presence of only plagioclase in the host rock; in terms of the degree of weathering in provenance areas without potassium feldspar, the larger the PIA value is, the stronger the degree of weathering (Xu et al 2018; Zhao et al 2019). Fig. 4 shows that the values of CIA, CIW, and PIA are in the ranges of 6.83-64.64, 7.01-70.15, and 3.82-20.38, respectively; the range variations indicate that the weathering degrees of the PWR samples obtained at different outcrops were quite different.

4 **Engineering geological properties**

4.1 Methodology

The physical and mechanical properties of PWR in the K_1/J_2 contact zone are tested in accordance with the "Standard for test methods of engineering rock mass" (China EC 2013). The tested physical and mechanical properties of PWR include the water content, bulk density, real density, porosity, longitudinal wave velocity, expansion rate, PLS and UCS. Rocks exhibit different engineering properties under different water content states (Majeed et al 2018). To gain a better understanding of the original properties of PWR, this paper tested the water content of the PWR samples in their natural state and calculated it by Eq. (1):

$$\mathrm{w} = \frac{m_o - m_s}{m_s} \times 100 \qquad (1)$$

where w (%) is the water content of the rock, m_o (g) is the sample mass before drying, and m_s (g) is the sample mass after drying.

Density, defined as mass divided by volume, is the basic property of rock (Miller 1965) and is closely related to the geotechnical properties of the rock. The volume measurement includes or excludes the voids inside the rock, referred to as the bulk and real density, respectively. The bulk density is tested by the wax sealing method and calculated according to Eq. (2):

$$\rho_{bluk} = \frac{m_s}{\frac{m_1 - m_2}{\rho_w} - \frac{m_1 - m_s}{\rho_p}} \qquad (2)$$

where ρ_{bluk} (g/cm^3) is the bulk density, m_s (g) is the drying mass of the bulk sample, m_1 (g) is the mass of the sealed test piece in air, m_2 (g) is the mass of the sealed test piece in water, ρ_w (g/cm^3) is the density of water (0.998 g/cm^3 at 20 e , and ρ_p (g/cm^3) is the density of paraffin wax.

The real density is determined with the pycnometer method and is calculated according to Eq. (3):

$$\rho_r = \frac{m_s}{m_1 + m_s - m_2} \times \rho_{WT} \qquad (3)$$

where ρ_r (g/cm^3) is the real density; m_s (g) is the drying mass of the powdered sample; m_1 (g) is the total mass of the bottle and test solution; m_2 (g) is the total mass of the bottle, test solution and rock powder; and P_{WT} (g/cm^3) is the density of the test solution, which is the same as the test temperature.

Porosity is one of the important physical properties that control the mechanical properties of rock strength and deformability (Palchik and Hatzor 2002; Sabatakakis et al. 2008; Pappalardo 2015). The

total porosity (n) is the ratio of pore volume to sample volume and is calculated according to Eq. (4):

$$n = (1 - \frac{\rho_{bluk}}{\rho_r}) \times 100 \qquad (4)$$

where n (%) is the total porosity, ρ_{bluk} (g/cm^3) is the bulk density, and ρ_r (g/cm^3) is the real density.

The speed at which ultrasonic waves propagate in the rock depends on the density of the rock and the pores and cracks in the rock (Khandelwal et al. 2010). A UTA-2000 intelligent ultrasonic detector measuring instrument was used to test the longitudinal wave velocity V_p of the PWR; the sampling frequency was 10 MHz, and the timing accuracy was 0.1 s. During the test, butter was applied to both ends of the rock sample to better couple the acoustic sensor with the sample. V_p was determined by dividing the length of the sample by the time required for the pulse to pass through the sample and was calculated according to Eq. (5):

$$v_p = \frac{L}{t_p - t_0} \qquad (5)$$

where v_p (m/s) is the longitudinal wave velocity, t_p (s) is the propagation time of the longitudinal wave in the direct transmission method, and t_0 (s) is the zero delay of the instrumental system.

Rock expansion refers to the expansion of rock volume with time under the action of external factors. There are many external factors that affect rock swelling: water penetration, reduction in rock external force, chemical substances (such as sulfide), frost action, etc. (Sun et al. 2013). The PWR in the K_1/J_2 contact zone studied in this paper is located under a thick Cretaceous water body; the thickness is mainly due to the expansion of the rock caused by the penetration of water. The expansion rate of the PWR was investigated through free expansion rate testing of the rock and was calculated according to Eq. (6):

$$V_H = \frac{\Delta H}{H} \times 100 \qquad (6)$$

where V_H (%) is the axial free expansion rate of the rock, $\triangle H$ (mm) is the axial deformation of the specimen, and H (mm) is the height of the specimen.

The point load test equipment used is a YXDZ-10 rock point load tester (maximum pressure of 10 kN) and a Vernier caliper (Fig. 5). The sample was collected and prepared to avoid cracks. The size of each irregular block specimen was 50 mm±35 mm, and the ratio of the distance between the two loading points to the average width of the loading point was 0.3-1.0. In the test, the direction of the minimum size of the test piece was selected as the loading direction. First, the instrument was checked to ensure accurate alignment, then the center of the sample was placed close contact with the loading cone. The pressure was adjusted to zero, and within 10-60 s, a load was applied at a constant speed until the specimen broke. The pressure gauge reading F at the time of failure was recorded, and the size of the broken surfaces of the specimen were measured.

According to the standard procedure of ASTM (1995), the formula for calculating the PLS of rock without size correction is as follows:

$$I_s = \frac{P}{D_e^2} \qquad (7)$$

where P (kN) is the applied load at failure and D_e (mm) is the equivalent diameter defined. For the diametral test, the calculation formula of equivalent core diameter D_e is as follows:

$$D_e = (D \times D')^{0.5} \qquad (8)$$

where D (mm) is the distance between two loading points and D' (mm) is the distance between loading points at the moment of specimen failure after penetration of the upper and lower cone ends. For axial and irregular lump tests, the calculation formula of equivalent core diameter D_e is as

follows:

$$D_e = (4lW \times D' / \pi)^{0.5} \quad (9)$$

where W (mm) is the average width of the minimum section through two loading points.

When the equivalent core diameter is not 50 mm, the PLS index of rock should be corrected. When there are many experimental data and the equivalent core diameter in the same group of samples has multiple sizes not equal to 50 mm, the relationship curve between D_e^2 and failure load P should be drawn based on the experimental results, and the corresponding P_{50} value when D_e^2 is 2500 mm^2 should be found from the curve. The PLS of the rock was calculated as follows:

$$I_{s(50)} = \frac{P_{50}}{2500} \quad (10)$$

where $I_{s(50)}$ (MPa) is the PLS index of the rock with an equivalent core diameter of 50 mm and P_{50} (kN) is the corresponding P value when D_e^2 is 2500 mm^2, as calculated from the P-D_e^2 relationship curve.

Fig. 5 shows the definitions of L, D, D', W_1 and W_2 (the widths at the upper and lower ends of the cross-section). Note that the average width W is defined as W= (W_1+W_2)/2. The dimension L is measured from the loading point to the nearest free face. The shape of the irregular lump samples strictly followed the ASTM (1995) standard, which suggests that the D/W ratio should be between 0.3 < D/W < 1 and that L should be $\geqslant 0.5D$. If the measured L, D and W do not meet this requirement, the test is invalidated, and the data are discarded. In addition, if the failure section does not pass through the loading points, the specimen is invalidated. Furthermore, all the samples must be checked to have an equivalent size greater than 10 times the mineral grains; otherwise, the test is also invalidated.

The experimental instrument used in this test was a D-1000 electrohydraulic servo universal testing machine, with a maximum axial load of 1000 kN (Fig. 6). During each test, the test piece was placed in the center of the pressure plate of the testing machine, the ball seat was adjusted, and the two ends of the test piece were in even contact with the upper and lower pressing plates of the testing machine; then, loading at the rate of 0.5-1.0 MPa/s was performed until failure. The failure load (P) and the phenomena that occurred during the loading process were recorded. The UCS of the rock was calculated according to the failure load and the section area of the test piece. The calculation formula is as follows:

$$R_c = \frac{P}{A} \quad (11)$$

where R_c (MPa) is the rock UCS, P (kN) is the failure load, and A (mm^2) is the cross-sectional area of the rock specimen.

4.2 Physical–mechanical characterization

According to the above testing methodology, we obtained the physical and mechanical properties of the PWR in the K_1/J_2 contact zone (Table 1). The water content of the PWR from the different outcrops ranges between 3.86% and 10.23%, with an average of 7.66%. The bulk density is between 2.36 and 2.57, with an average of 2.43; the real density is between 2.61 and 2.69, which is relatively uniform, with an average of 2.64. The porosity is between 4.11 and 10.27, and the average is 8.22. The porosity is relatively high, which may be caused by weathering. The longitudinal wave velocity is between 0.78 and 3.82, and the average is 1.95. The expansion rate is between 12.1 and 51.8, and the average is 32.9.

According to the experimental results of the irregular sample PLS, the P-D_e^2 relationship curve was drawn, and the P-D_e^2 linear regression fitting curve formula of each group of irregular samples is shown in Table 2, which also shows the linear regression correlation coefficient r, the determination coefficient r^2, and the significance F value of the F test. Mathematical statistics theory (Chen et al. 2014) suggests that the correlation coefficient r expresses the linear correlation degree between X and Y as two random variables, -1≤r≤a: when -1≤r<0, X and Y are negatively correlated; when r=0, X and Y are not correlated; and when 0<r≤hen$X$ and Y are positively correlated. The coefficient of determination r^2 indicates the degree of fit of a straight line and indicates how well the fitted straight line can reflect the fluctuation in Y, 0<r^2≤n: an r^2 value closer to 1 indicates a better fit. The F test was used to determine the linear significance of all independent variables X to Y as a whole; the significance F value is generally less than 0.05, and the smaller the value, the more significant it is (0.05 is actually the significance level, which was artificially set). In Table 2, the JB-1 group data show r=0.95>0, indicating that P and D_e^2 are positively correlated; r^2=0.9, which is close to 1, indicating a good degree of fit; and the significance F=5.29E-8<0.05, indicating that for all the samples, D_e^2 is linearly significant for P overall. Then, the P_{50} value corresponding to D_e^2=2500 mm was calculated according to the linear regression fitting formula for each group (Table 2), and the PLS index $I_{s(50)axi}$ of each group of irregular samples was calculated according to Eq. (4) (Table 1). The obtained irregular sample PLS is between 1.13-6.61, with an average of 2.64.

According to Eqs. (7)-(9), the axial and diametral PLSs were calculated (Table 1). The axial loaded PLS is between 2.65 and 13.41, with an average value of 5.97; the diametral loaded PLS is between 1.78 and 8.38, and the average value is 3.96. Table 1 shows that for the same group of samples with the same lithology, $I_{s(50)axi}$ >$I_{s(50)dia}$ >$I_{s(50)irr}$ because the direction of the axial point load is approximately perpendicular to the sedimentary layer of the sample, and the loading direction of the diametral point load is approximately parallel to the sedimentary bedding surface, which results in $I_{s(50)axi}$ > $I_{s(50)dia}$. This result is consistent with the research results of Basu et al (2010). The diametral and axial PLS tests are performed in the dry state, and the irregular sample PLS is tested in the natural moisture state. The PLS of the dry sample is higher than that of the water-containing sample (Jeng et al. 2004; Deng et al. 2019; Majeed et al. 2018), and the experimental results are consistent with the research results of Hawkins (1998). According to Eq. (5), the UCS of the PWR was calculated (Table 1) to be between 13.65 and 160.69. The degree of variation in UCS is large, which may be caused by the variation in lithology, cement and degree of weathering; the average UCS is 73.61.

5. Discussion

5.1 Correlations between engineering geological and petrographic properties of PWR

Rocks are composed of mineral aggregates (including crystalline and amorphous minerals) with a certain structure. Therefore, the mechanical properties of fresh rock mainly depend on the mineral composition and relative content of the rock (Liu et al. 1999). Some scholars believe that rock strength is linearly related to mineral composition and content (Fereidooni 2016; Wang et al. 2019; Pappalardo et al. 2016), while others believe that rock strength is exponentially related to mineral composition and content (Meng et al. 2007; Pappalardo et al. 2016). As shown in Fig. 3, each group of samples contains quartz, while the other minerals present depend on the sampling location; this variability is caused by the different degrees of weathering in different locations. This work attempted to analyze the relationship between PLS, UCS and quartz content of PWR by linear regression and

exponential regression. The results show that the correlation coefficient of linear regression is higher than that of exponential regression; the linear regression formula is shown in Table 3, and the PLS and UCS of PWR are positively correlated with the content of quartz. According to the description of their petrological characteristics, calcite, quartz, dolomite, and albite are brittle and high in hardness and are collectively referred to as the BMG, while muscovite, clay minerals, and chlorite minerals are elastic and low in hardness and are collectively referred to as the EMG. We analyze the correlation between the strength of the PWR and the BMG and EMG contents, and the results are shown in Table 3. The PLS and UCS of the PWR are positively correlated with the BMG content and negatively correlated with the EMG content. We also tested the expansion rate of the PWR, and the content of clay minerals in the rock determines the PWR expansion rate. The expansion rate of the PWR is linearly positively correlated with the content of the clay minerals (Table 3).

When the rock undergoes weathering, primary minerals will transform into secondary minerals; at the same time, changes in the chemical composition and structure of the rock will lead to the gradual destruction of the rock. The higher the degree of weathering of the rock is, the more serious the degree of destruction, and the worse its mechanical properties. The main chemical elements of the PWR were analyzed by XRF, and three weathering alteration indexes were calculated (CIA, CIW, and PIA) (Fig. 4). We also analyzed the correlation between the strength of PWR and CIA, CIW, and PIA, and the results are shown in Fig. 7. The PLS and UCS of the PWR are negatively correlated with the three weathering alteration indexes, and the correlations between the PLS and the three weathering alteration indexes are higher than those between the UCS and the three indexes.

5.2 Correlations between the mechanical and physical properties of PWR

The mechanical properties of rock are affected by its water content. Jeng et al. (2004) and Deng et al. (2019) studied the influence of water content on the strength of sandstone and found that water saturation and wetting will cause the strength of sandstone to decrease. Majeed et al. (2018) studied the influence of water content on the strength of sedimentary rocks and found that the UCS of saturated rock is 40%-50% lower than that of dry rock. Wei et al. (2020) studied the influence of water content on the strength of gypsum and found that an increasing water saturation had a weakening effect on the strength of gypsum. The results of the correlation analysis of the strength and water content of the PWR in this paper are shown in Fig. 8. The PLS and water content of the PWR are negatively exponentially correlated, UCS is negatively linearly related to the moisture content, and an increasing water saturation reduces the strength of the PWR. Some scholars believe that the correlation between rock strength and density is linear (Chatterjee 2002; Fereidooni 2016; Aligholi et al. 2019), while others believe it is exponential (Wang et al. 2019). In this paper, the correlation analysis results of the PWR strength and the bulk density and real density are shown in Fig. 8. The PLS is positively exponentially correlated with the bulk density and real density, and the UCS is positively linearly correlated with the bulk density and real density. Porosity is one of the important parameters that controls rock strength (Pappalardo 2015). The PLS and total porosity of the PWR are negatively exponentially correlated, and the UCS is negatively linearly related to total porosity (Fig. 8). These findings are consistent with previous research results (Chatterjee 2002; Fereidooni 2016; Wang et al. 2019; Dincer et al. 2004). Some scholars have studied the relationship between rock strength and longitudinal wave velocity, finding that some relationships are linear (Fereidooni 2016; Pappalardo et al. 2016; Aligholi et al. 2019) while others are exponential (Wang et al. 2019). In this paper, there is an positive exponential correlation between the PLS and the longitudinal wave velocity,

and the UCS has a positive linear correlation with the longitudinal wave velocity (Fig. 8).

5.3 Correlation between the PLS and UCS of PWR

This section describes the regression analysis conducted on the PLS and UCS data of the PWR in the K_1/J_2 contact zone and the relationship between them, providing a theoretical basis with which engineers can use point load tests to quickly estimate the UCS of PWR in practical engineering applications. There are many studies on the correlation between rock PLS and UCS. Most scholars believe that UCS and PLS are linearly related (D'Andrea et al. 1965; Broch et al. 1972; Gunsallus et al. 1984; Hawkins 1998; Kahraman 2001; Palchik et al. 2004; Sabatakakis et al. 2008; Basu et al. 2010; Xiang 1981; Wei 1982; Li et al. 2013; Liu et al. 2019), and a few scholars believe that UCS and PLS are exponentially related (Quane 2003; Robina 2015). We conducted a linear regression analysis on the relationships between the UCS and the PLS, axial PLS, diametral PLS and irregular PLS, and the results are shown in Fig. 9; all the relationships show a positive linear correlation.

Whether the UCS obtained from the transformation of the PLS test is accurate and reliable is discussed next. In this paper, the relative error between the UCS obtained from the transformation of the PLS test and the UCS of standard laboratory rock samples is used for verification. The definition of the relative error is as follows (Wang 2015):

$$\delta : \frac{|R_c - \sigma_c|}{\sigma_c} \times 100\% \qquad (7)$$

where R_c is the UCS obtained from PLS test conversion and σ_c is the UCS of the standard laboratory rock sample.

The calculated relative errors of UCS obtained by the PLS relation and ISRM method are shown in Table 4. Using the method described in this paper, the relative error ranges between the UCS values estimated by the PLS testing of samples (irregular, diametral, and axial) and the measured values obtained by standard laboratory rock UCS testing are 0.38%-10.12%, 0.91%-13.22%, and 0.25%-7.03%, respectively; the average values are 3.13%, 6.02%, and 2.79%, respectively. Using the ISRM method, the relative error range between the UCS of PWR samples estimated by the PLS testing of samples (irregular, diametral, and axial) and the measured values obtained by the laboratory standard rock UCS testing are 17.91%-101.42%, 13.89%-108.67%, and 0.15%-30.31%, and the average values are 48.95%, 54.21%, and 9.83%, respectively. By comparison, the method in this paper is more reasonable than the ISRM method, and the error of the estimated UCS is smaller, which is more suitable for the transformation between the PLS and UCS values of the PWR in the K_1/J_2 contact zone of the Ordos Basin.

6. Conclusions

Experimental analysis of complete rock blocks is one of the main basic problems that need to be solved in rock mass research (Bieniawski 1989). Therefore, a detailed description of the geological characteristics of the rock blocks affected by a project is of great significance to the study of the physical and mechanical properties of the rock mass.

For this research, laboratory tests were conducted on PWR samples from the K_1/J_2 contact zone of the Ordos Basin to study the petrological and engineering geological characteristics of PWR, analyze the impact of the petrological and physical characteristics of PWR on its mechanical properties, and ensure the safe implementation of PWR engineering activities in the K_1/J_2 contact zone in the Ordos Basin.

From the hand-scale analysis, the PWR is massive, with sandy gravel, fine-grained and muddy

structures, occasionally black and white cryptocrystalline, and can be observed as irregular rock blocks, occasionally with fine cracks.

From a mineralogical point of view, 9 minerals, including quartz, calcite, dolomite, albite, muscovite, kaolinite, illite, montmorillonite and chlorite were detected in the studied PWR, but only quartz is constantly present. The presence of other minerals vary depending on the sampling location and the degree of weathering. A total of 7 types of oxides were detected in the PWR; each group of samples contained Fe_2O_3, which had been decomposed into amorphous iron, and chlorite was not detected in some groups of samples. The values of the three weathering alteration indexes (CIA, CIW, and PIA) vary widely, indicating that the degree of weathering of the PWR varies greatly.

From a physical point of view, the real density of the PWR is relatively uniform. After long-term weathering, the porosity is relatively high. The existence of clay minerals causes the PWR to have a certain expansion rate.

From a mechanical point of view, the PWR is irregular, the axial and diametral PLSs are relatively close, and for the same group of samples with the same lithology, $I_{s(50)axi} > I_{s(50)dia} > I_{s(50)irr}$. The UCS of the PWR has a wide range. Notably, the UCS of each group of samples is determined in accordance with the "Standard for test methods of engineering rock mass". Therefore, the experimental results and relationships can be considered reliable for the characterization of rock types.

The mineralogical, physical and mechanical properties of the PWR were compared to predict one parameter from another and study their mutual influence.

The relationships between the PLS and UCS of the PWR and the content of quartz minerals were studied, and the results show positive linear trends. According to the petrological description, calcite, quartz, dolomite and albite are collectively referred to as the BMG, and muscovite, clay minerals and chlorite minerals are collectively referred to as the EMG. The PLS and UCS of the PWR are linearly positively correlated with the BMG and EMG, respectively. Brittle minerals have greater hardness, so the higher their content is in the PWR, the greater its PLS and UCS; the higher the content of elastic minerals is, the lower the PLS and UCS. This result is a new aspect of rock behavior prediction. The expansion rate of PWR is linearly positively correlated with the content of clay minerals. The PWR swells when in contact with water and becomes muddy, which explains the water (mud) inrush accidents of the coal mines in the study area. This PWR has experienced weathering for a long time, and changes in mineral composition, chemical composition and structure have led to the deterioration of its rock mechanical properties; the PLS and UCS of the PWR are negatively correlated with the three weathering alteration indexes (CIA, CIW, and PIA).

The relationships between the strength of the PWR and its physical characteristics are studied. The results show that the PLS is negatively correlated with the water content and total porosity and positively correlated with the bulk density, real density, and longitudinal wave velocity. The UCS has a negative linear correlation with the water content and total porosity, as well as a positive linear correlation with the bulk density, real density and longitudinal wave velocity.

The relationship between UCS and PLS was studied, and the results show that UCS and PLS have a positive linear correlation; additionally, the axial and diametral PLSs and irregular PLS also show a positive linear correlation. This research result provides a theoretical basis for engineers to quickly estimate the UCS and PLS of regular samples by using irregular rock block point load tests in practical engineering applications.

Acknowledgement: The study was supported by the State Key Program of the National Natural

Science Foundation of China (Grant 41931284).

References

ASTM (1995) Standard test method for determination of the point load strength index of rock and application to rock strength classification. Test Designation D5731-95 Annual book of ASTM standards. Philadelphia: American Society for Testing and Materials.

Basu A, Kamran M (2010) Point load test on schistose rocks and its applicability in predicting uniaxial compressive strength. Int J Rock Mech Min 47:823-828. https://doi.org/10.1016/j.ijrmms.2010.04.006

Bieniawski ZT (1989) Engineering rock mass classification. Wiley, New York.

Broch E, Franklin JA (1972) The point-load strength test. Int J Rock Mech Min 9:669-676. https://doi.org/ 10.1016/0148-9062(72)90030-7

Cantisani E, Garzonio CA, Ricci M, Vettori S (2013) Relationships between the petrographical, physical and mechanical properties of some Italian sandstones. Int J Rock Mech Min 60:321-332. https://doi.org/10.1016/j.ijrmms.2012.12.042

Chatterjee R, Mukhopadhyay M (2002) Petrophysical and geomechanical properties of rocks from the oilfields of the Krishna Godvari and Cauvery Basins, India. B Eng Geol Environ 61:169–178. https://doi.org/10.1007/s100640100137

Chen ZT, Zhao DP, Li YP, Pan DS (2014) Mathematical Statistics. National defense industry press, Beijing.

China EC (2013) Standard for test methods of engineering rock mass. China planning press, Beijing.

D'Andrea DV, Fogelson DE, Fisher RL (1965) Prediction of compression strength from other rock properties. U.S. Dept. of the Interior, Bureau of Mines, Washington.

Dincer I, Acar A et al (2004) Correlation between Schmidt hardness, uniaxial compressive strength and Young's modulus for andesites, basalts and tuffs. Bull Eng Geol Env 63:141-148. https://doi.org/10.1007/s10064-004-0230-0

Douma LANR, Primarini MIW, Houben ME, Barnhoorn A (2017) The validity of generic trends on multiple scales in rock-physical and rock-mechanical properties of the Whitby Mudstone, United Kingdom. Mar Petrol Geol 84:135-147. https://doi.org/10.1016/j.marpetgeo.2017.03.028

Elena S, Lyalya S, Victor I, 2015. The major types of the weathering crust of the eastern Russian plate and its mineralogical and geochemical features. Procedia Earth Planet Sci 573-578. https://doi.org/10.1016/j.proeps.2015.08.105

Farkas O, Siegesmund S, Licha T, 2018. Geochemical and mineralogical composition of black weathering crusts on limestones from seven different European countries. Environ Earth Sci 77:211. https://doi.org/10.1007/s12665-018-7384-8

Fereidooni D (2016) Determination of the geotechnical characteristics of hornfelsic rocks with a particular emphasis on the correlation between physical and mechanical properties. Rock Mech Rock Eng 49, 2595-2608. https://doi.org/10.1007/s00603-016-0930-3

Gunsallus KL, Kulhawy FH (1984) A comparative evaluation of rock strength measures. Int J Rock Mech Min 21:233-248. https://doi.org/10.1016/0148-9062(84)92680-9

Guo XM, Guo K, Liu YF (2020) Multi-source information evaluation of mud and sand inrush disaster during the mining of deep-buried coal seam. Coal Geol Explor 48:113-119,128. https://doi.org/10.3969/j.issn.1001-1986.2020.01.015

Han LF, Bai ZD (2020) Volcanic geological features and geochemical implications of Late Jurassic

volcanoes in Duolun volcanical features and geochemical implications oGeol J 3. https://doi.org/10.1002/gj.3973

Hawkins AB (1998) Aspects of rock strength. Bull Eng Geol Environ 57:17-30. https://doi.org/10.1007/s100640050017

Heidari M, Khanlari GR, Kaveh MT, Kargarian S (2012) Predicting the uniaxial compressive and tensile strengths of gypsum rock by point load testing. Rock Mech Rock Eng 45:265-273. https://doi.org/10.1007/s00603-011-0196-8

Huang DY, 2019. Jurassic integrative stratigraphy and timescale of China. Sci China Earth Sci 62: 223-255. https://doi.org/10.1007/s11430-017-9268-7

Jia CZ, Wei GQ, Li BL (2005) Yanshanian tectonic features in west-central China and their petroleum geological significance. Oil Gas Geol 26:9-15. https://doi.org/10.3321/j.issn:0253-9985.2005.01.003

Kahraman S (2001) Evaluation of simple methods for assessing the uniaxial compressive strength of rock. Int J Rock Mech Min 38:981-994. https://doi.org/10.1016/S1365-1609(01)00039-9

Khandelwal M, Ranjith PG (2010) Correlating index properties of rocks with P-wave measurements. J Appl Geophys 71:1-5. https://doi.org/10.1016/j.jappgeo.2010.01.007

Li DY, Wong LNY (2013) Point load test on meta-sedimentary rocks and correlation to UCS and BTS. Rock Mech Rock Eng 46:889-896. https://doi.org/10.1007/s00603-012-0299-x

Lin ZY (1996) Geotechnical investigation and design manual. Liaoning science and technology press, Liaoning.

Liu QS, Zhao YF, Zhang XP (2019) Case study: using the point load test to estimate rock strength of tunnels constructed by a tunnel boring machine. Bull Eng Geol Environ 78:1727-1734. https://doi.org/10.1007/s10064-017-1198-x

Lu QY, Li XQ, Li WP, Chen WC, Li LF, Liu SL (2018) Risk evaluation of bed-separation water inrush: a case study in the Yangliu Coal Mine, China. Mine Water Environ 37:288-299. https://doi.org/10.1007/s10230-018-0535-z

Majeed Y, Bakar MZA (2018) Water saturation influences on engineering properties of selected sedimentary rocks of Pakistan. J Min Sci 54:914-930. https://doi.org/10.1134/S1062739118065060

Marques EAG, Williams DJ, Assis IR, Leão MF (2017) Effects of weathering on characteristics of rocks in a subtropical climate: weathering morphology, in situ, laboratory and mineralogical characterization. Environ Earth Sci 76:602. https://doi.org/10.1007/s12665-017-6936-7

Menningen J, Siegesmund S, Lopes L, Martins R, Sousa L (2018) The Estremoz marbles: an updated summary on the geological, mineralogical and rock physical characteristics. Environ Earth Sci 77:191. https://doi.org/10.1007/s12665-018-7328-3

Meng Z, Pan J (2007) Correlation between petrographic characteristics and failure duration in clastic rocks. Eng Geol 89:258-265. https://doi.org/10.1016/j.enggeo.2006.10.010

Miller RP (1965) Engineering classification and index properties for intact rock. Dissertation, University of Illinois.

Palchik V, Hatzor YH (2002) Crack damage stress as a composite function of porosity and elastic matrix stiffness in dolomites and limestones. Eng Geol 63:233–245. https://doi.org/10.1016/S0013-7952(01)00084-9

Palchik V, Hatzor YH (2004) The influence of porosity on tensile and compressive strength of porous chalks. Rock Mech Rock Eng 37:331-341. https://doi.org/10.1007/s00603-003-0020-1

Pappalardo G (2015) Correlation between P-wave velocity and physical–mechanical properties of intensely jointed dolostones, Peloritani mounts, NE Sicily. Rock Mech Rock Eng 48:1711–1721. https://doi.org/10.1007/s00603-014-0607-8

Pappalardo G, Punturo R, Mineo R, Ortolano G, Castelli F (2016) Engineering geological and petrographic characterization of migmatites belonging to the calabria-peloritani orogen (southern Italy). Rock Mech Rock Eng 49:1143-1160. https://doi.org/10.1007/s00603-015-0808-9

Quane SL (2003) Russell JK. Rock strength as a metric of welding intensity in pyroclastic deposits. Eur J Mineral 15:855-864. https://doi.org/10.1127/0935-1221/2003/0015-0855

Sabatakakis N, Koukis G, Tsiambaos G, Papanakh S (2008) Index properties and strength variation controlled by microstructure for sedimentary rocks. Eng Geol 97:80-90. https://doi.org/10.1016/j.enggeo.2007.12.004

Shaldybin MV, Wilson MJ, Wilson L et al (2019) A kaolinitic weathering crust in Tomsk, West Siberia: Interpretation in the context of weathering crusts in Russia and elsewhere Catena 181. https://doi.org/10.1016/j.catena.2019.05.002

Sousa LMO et al. (2005) Influence of microfractures and porosity on the physico-mechanical properties and weathering of ornamental granites. Eng Geol 77:153–168. https://doi.org/10.1016/j.enggeo.2004.10.001

Sun Q, Qing SQ, Su TM et al (2013) Engineering geological effects of rock weathering. China university of mining and technology press, Xuzhou.

Sun WJ, Wang LB, Wang YQ (2017) Mechanical properties of rock materials with related to mineralogical characteristics and grain size through experimental investigation: a comprehensive review. Front Struct Civ Eng 11:322-328. https://doi.org/10.1007/s11709-017-0387-9

Tamrakar NK, Yokota S, Shrestha SD (2007) Relationships among mechanical, physical and petrographic properties of Siwalik sandstones, Central Nepal Sub-Himalayas. Eng Geol 90:105–123. https://doi.org/10.1016/j.enggeo.2006.10.005

Ulyasheva N, Grakova O, Pystin A, Pystina Y (2016) Structural and compositional characteristics of the rocks of the Nyarovey series (Polar Urals). WMESS 44:052067 https://doi.org/44:052067. 10.1088/1755-1315/44/5/052067

Undul, Omer (2016) Assessment of mineralogical and petrographic factors affecting petro-physical properties, strength and cracking processes of volcanic rocks. Eng Geol 210:10-22. https://doi.org/10.1016/j.enggeo.2016.06.00

Vikram G, Ruchika S (2012) Relationship between textural, petrophysical and mechanical properties of quartzites: a case study from northwestern Himalaya. Eng Geol 135–136:1–9. https://doi.org/10.1016/j.enggeo.2012.02.006

Vonto DC et al. (2020) Geology and geotechnical characteristics of the Gbago and Ngouaka plutonic rocks, North East of Bangui, Central Africa Republic. J Afr Earth Sci 167. https://doi.org/10.1016/j.jafrearsci.2020.103831

Wang CC (2015) Selection of uniaxial compressive strength from point load tests for irregular rock specimens. Geotech Invest Surv 43:19-22. https://doi.org/ JournalArticle/5b3b7009c095d70f007502c6

Wang JM, 2011. karst Palaeogeomorphology and reservoir characteristics of Ordovician weathered crust in eastern Ordos Basin. Dissertation, Northwest University.

Wang ZK, Li WP et al (2019) Relationships between the petrographic, physical and mechanical characteristics of sedimentary rocks in Jurassic weakly cemented strata. Environ Earth Sci

78:131. https://doi.org/10.1007/s12665-019-8130-6
Wei KH (1982) Study on quantitative evaluation of weathering degree of granite by point load method. Hydro Eng Geol 2:28-31. https://doi.org/CNKI:SUN:SWDG.0.1982-02-007
Wei SJ, Wang CY, Yang YS, Wang M (2020) Physical and mechanical properties of gypsum-like rock materials. Adv Civ Eng 1:1-17. https://doi.org/10.1155/2020/3703706
Wong RHC, Chau KT, Yin JH, Lai dtw, Zhao GS (2017) Uniaxial compressive strength and point load index of volcanic irregular lumps. Int J Rock Mech Min 93:307-315. https://doi.org/10.1016/j.ijrmms.2017.02.010
Xiang GF (1981) Comparative study on rock point load test. Hydro Eng Geol 1:45-48. https://doi.org/CNKI:SUN:SWDG.0.1981-01-010
Xu H, Liu YQ, Kuang HW et al (2013) Sedimentology，palaeogeography and palaeoecology of the Late Jurassic-Early Cretaceous eolian sands in north China. J Palaeogeo 15:11-30. https://doi.org/10. 7605/gdlxb.2013.01.002
Xu XT, Shao LY (2018) Limiting factors in utilization of chemical index of alteration of mudstones to quantify the degree of weathering in provenance. J Palaogeog 20:515-522. https://doi.org/10.7605/gdlxb.2018.03.038
Zhao P, Li AM, Li ST et al (2019) The REE geochemical characteristics of the basalt weathering crust in the northwestern Guizhou. Acta Mineralogica Sinica 39:464-473. https://doi.org/10.16461/j.cnki.1000-4734.2019.39.058
Zhang YF, Zhao H, Yuan HQ, Gao ZH (2013) Clastic rock physical characteristics of southern songliao basin shiwu fault depression layer. Adv Mater Res 838-841:1311-1315. https://doi.org/10.4028/www.scientific.net/AMR.838-841.1311
Zhang YQ, Liao CZ, Shi W, et al (2007) On the Jurassic deformation in and around the Ordos Basin, North China. Earth Sci Front 14:182-196. https://doi.org/10.3321/j.issn:1005-2321.2007.02.015
Zhu TE, Li WP, Wang QQ, Hu YB, Fan KF, Du JF (2020) Study on the height of the mining-induced water-conducting fracture zone under the Q_{21} loess cover of the Jurassic coal seam in northern Shaanxi, China. Mine Water Environ 39:57–67. https://doi.org/10.1007/s10230-020-00656-z

List of figure and table captions:

Fig.1 Location of study area: **a** Field outcrop survey sites, **b** Typical outcrop profile.

Fig.2 photos of the PWR macroscopic and microscopic featutes.

Fig.3 Mineral compositions of the PWR.

Fig.4 Main element contents and alteration weathering index of the PWR.

Fig.5 Point load instrument (YXDZ-10) and the definitions of L, D, D', W_1 and W_2.

Fig.6 D-1000 electro-hydraulic servo universal testing machine.

Fig.7 Relationships between strength of PWR and CIA, CIW, and PIA.

Fig.8 Relationships between strength of PWR and physical properties.

Fig.9 Relationships between the UCS and PLS, axial PLS, diametral PLS and irregular PLS.

Table 1 Physical and mechanical properties of the PWR in the K_1/J_2 contact zone

Sample groups	Water content (%) mean/times	Bulk density (g/cm^3)	Real density (g/cm^3)	Total porosity (%)	V_p (Km/s)	Expansion rate (%)	$I_{s(50)}$ (Mpa)			UCS (Mpa)
							irregular	axial	diameter	
JB-1	7.06/5	2.41	2.63	8.37	2.83	—	2.82	7.78	4.45	105.31
JB-2	8.04/6	2.36	2.62	9.92	1.35	—	1.19	4.02	2.23	15.77
JB-3	8.66/6	2.36	2.61	9.58	1.23	—	1.15	3.42	2.16	14.87
JB-4	7.51/5	2.44	2.64	7.58	2.15	12.1	2.76	7.78	4.79	105.52
JB-5	5.97/6	2.49	2.66	6.39	2.24	15.6	3.69	8.37	6.49	135.69
JB-6	9.09/7	2.36	2.63	10.27	0.88	18.4	1.07	2.65	1.78	14.35
JB-7	4.81/6	2.55	2.69	5.21	3.42	—	4.23	11.02	6.89	139.77
JB-8	3.86/5	2.57	2.68	4.11	3.82	12.4	5.28	13.41	8.38	160.69
JB-9	7.15/5	2.39	**2.62**	8.78	1.96	50.5	2.1	4.81	3.49	86.2
JB-10	6.91/6	2.45	2.65	7.55	2.74	29	2.56	5.36	4.09	100.99
JB-11	7.32/5	2.4	2.63	8.75	1.83	48.1	1.81	4.19	2.99	71.85
JB-12	7.86/5	2.45	2.67	8.24	2.38	41.2	2.22	4.87	3.68	90.58
AS-1	8.89/6	2.43	2.65	8.31	1.71	25.4	1.86	4.25	3.39	81.98
GQ-1	9.32/6	2.39	2.63	9.13	1.57	31.5	1.75	4.15	2.96	62.13
GQ-2	10.23/6	2.38	2.62	9.16	1.25	44.3	1.13	3.75	2.41	14.56
SM-1	9.56/5	2.35	2.60	9.62	0.97	51.8	1.06	3.68	2.26	13.65
SM-2	9.15/6	2.4	2.63	8.75	0.78	49.8	1.35	3.94	2.63	37.35

Table 2 The *P-*D_e^2 regression equations and coefficient of determination

Sample groups	P-D_e^2 regression equation	r	r^2	Significance F
JB-1	P=0.2151+0.0027 D_e^2	0.95	0.9	5.29E-08
JB-2	P=0.0282+0.0012 D_e^2	0.83	0.69	6.22E-05
JB-3	P=-0.3143+0.0021 D_e^2	0.89	0.79	2.47E-05
JB-4	P=0.3775+0.0026 D_e^2	0.91	0.83	6.15E-06
JB-5	P=0.2851+0.0036 D_e^2	0.87	0.76	2.62E-05
JB-6	P=0.0285+0.0011 D_e^2	0.95	0.91	3.86E-08
JB-7	P=0.5816+0.004 D_e^2	0.96	0.92	5.46E-09
JB-8	P=1.4681+0.0047 D_e^2	0.9	0.81	4.65E-06
JB-9	P=2.3231+0.0012 D_e^2	0.92	0.85	9.23E-07
JB-10	P=0.0728+0.0025 D_e^2	0.87	0.76	2.03E-05
JB-11	P=-2.3877+0.0028 D_e^2	0.92	0.84	1.68E-06
JB-12	P=0.4701+0.0020 D_e^2	0.92	0.85	9.23E-07
AS-1	P=0.1258+0.0018 D_e^2	0.85	0.72	5.36E-06
GQ-1	P=0.8564+0.0014 D_e^2	0.91	0.83	3.24E-07
GQ-2	P=0.7496+0.0008 D_e^2	0.87	0.76	2.65E-06
SM-1	P=0.0598+0.0010 D_e^2	0.88	0.77	1.84E-07
SM-2	P=1.0247+0.0008 D_e^2	0.92	0.85	8.32E-05

Table 3 Regression equations and determination coefficient of PWR strength and mineral content

Regression equation	r	r^2	Significance F
$I_{s(50)irr}$=1.46+5.35 Qu	0.6	0.36	2.13E-03
$I_{s(50)axi}$=3.49+15.34 Qu	0.64	0.41	3.89E-03
$I_{s(50)dia}$=2.68+7.88 Qu	0.59	0.35	1.24E-03
UCS=45.33+193.61 Qu	0.66	0.44	4.53E-03
$I_{s(50)irr}$=3.23-1.78 EMG	-0.67	0.45	4.68E-03
$I_{s(50)axi}$=8.60-5.12 EMG	-0.71	0.51	1.23E-04
$I_{s(50)dia}$=5.34-2.70 EMG	-0.66	0.44	4.45E-03
UCS=107.56-60.64 EMG	-0.64	0.41	3.12E-03
$I_{s(50)irr}$=1.45+1.78 BMG	0.67	0.45	4.67E-03
$I_{s(50)axi}$=3.48+5.12 BMG	0.71	0.51	1.31E-04
$I_{s(50)dia}$=2.64+2.70 BMG	0.66	0.44	4.59E-03
UCS=46.93+60.64 BMG	0.62	0.39	2.98E-03
ER=0.03+0.70 CM	0.95	0.9	3.85E-07

Figures

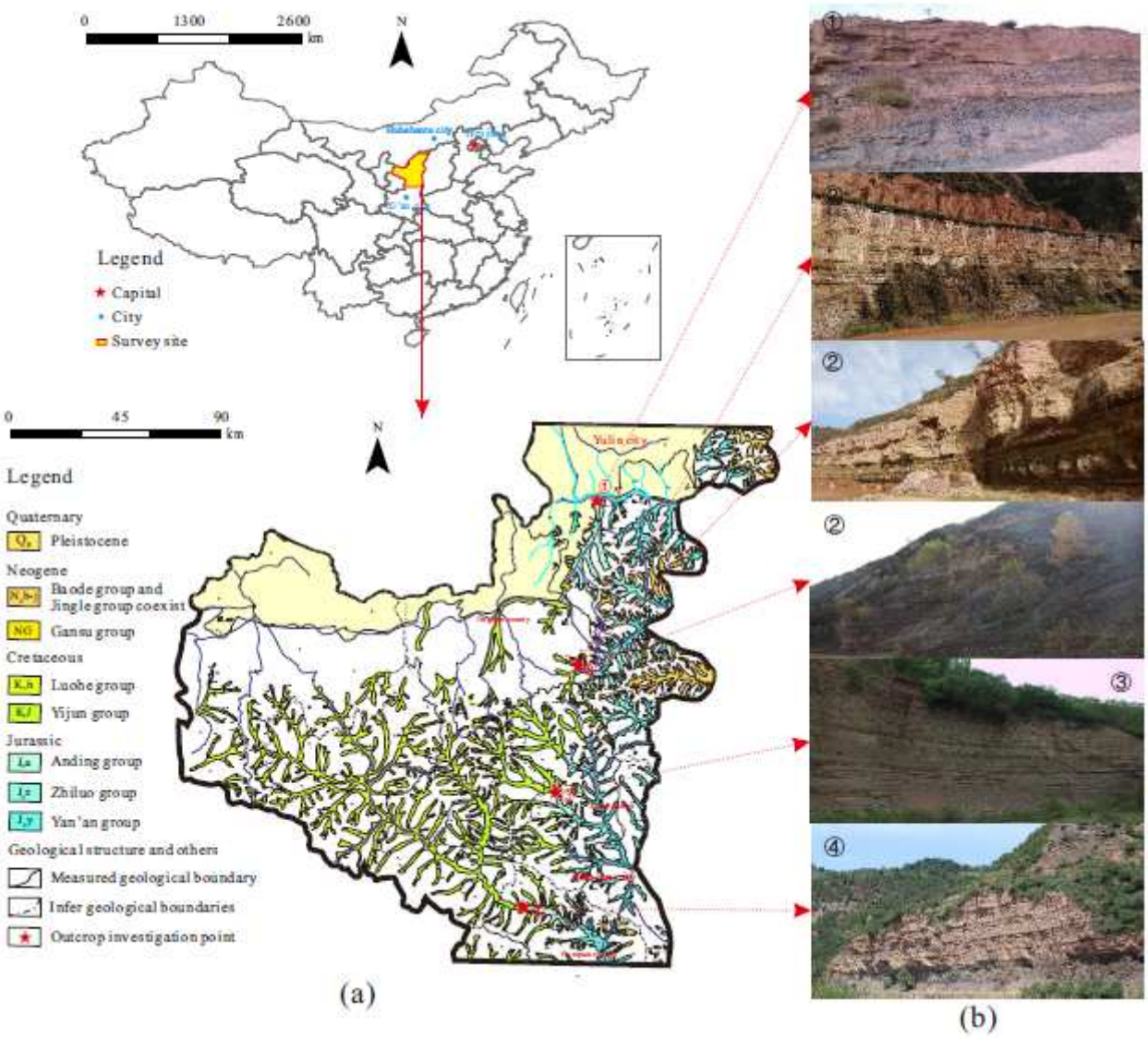

Figure 1

Location of study area: a Field outcrop survey sites, b Typical outcrop profile. Note: The designations employed and the presentation of the material on this map do not imply the expression of any opinion whatsoever on the part of Research Square concerning the legal status of any country, territory, city or area or of its authorities, or concerning the delimitation of its frontiers or boundaries. This map has been provided by the authors.

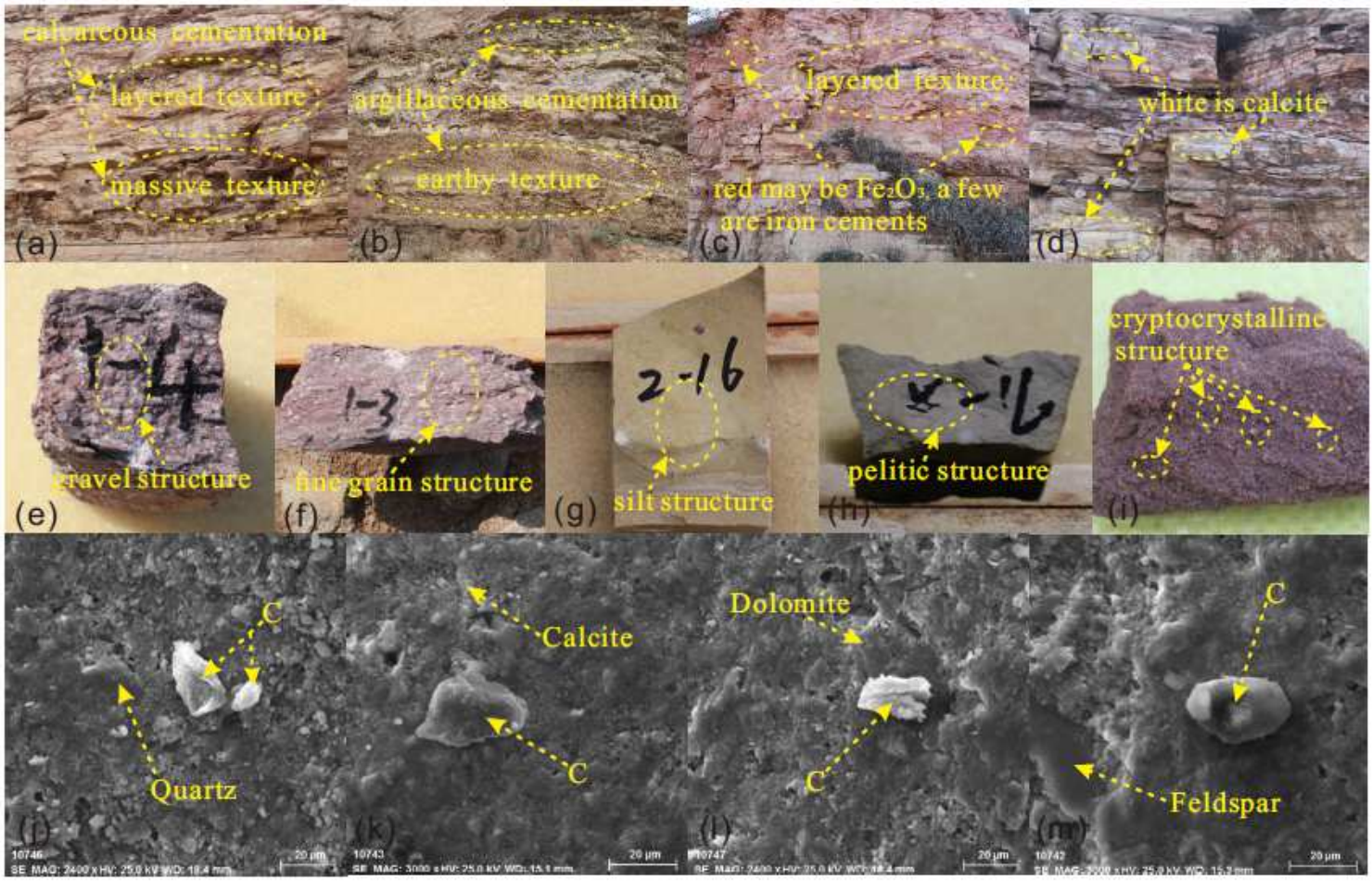

Figure 2

photos of the PWR macroscopic and microscopic featutes.

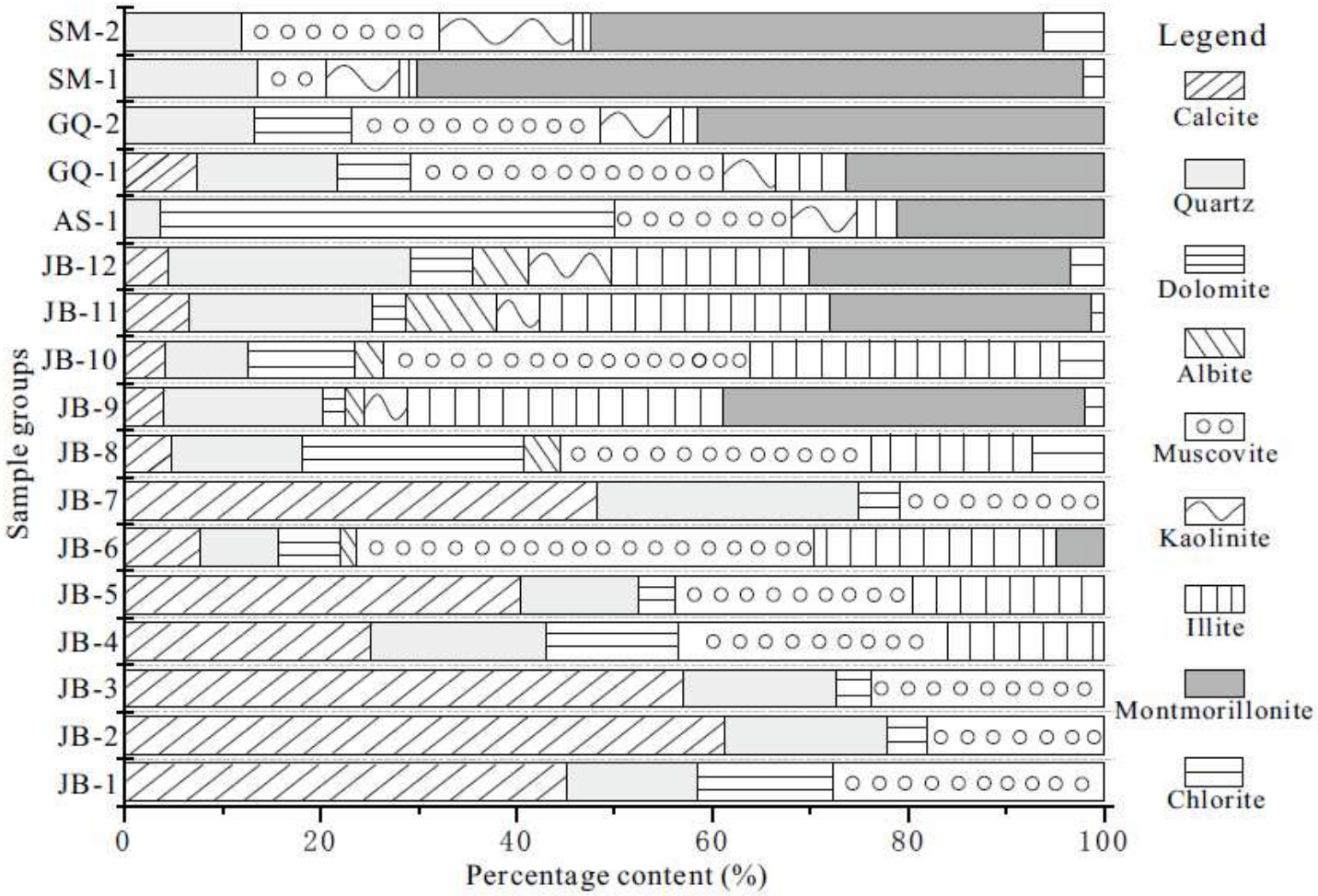

Figure 3

Mineral compositions of the PWR.

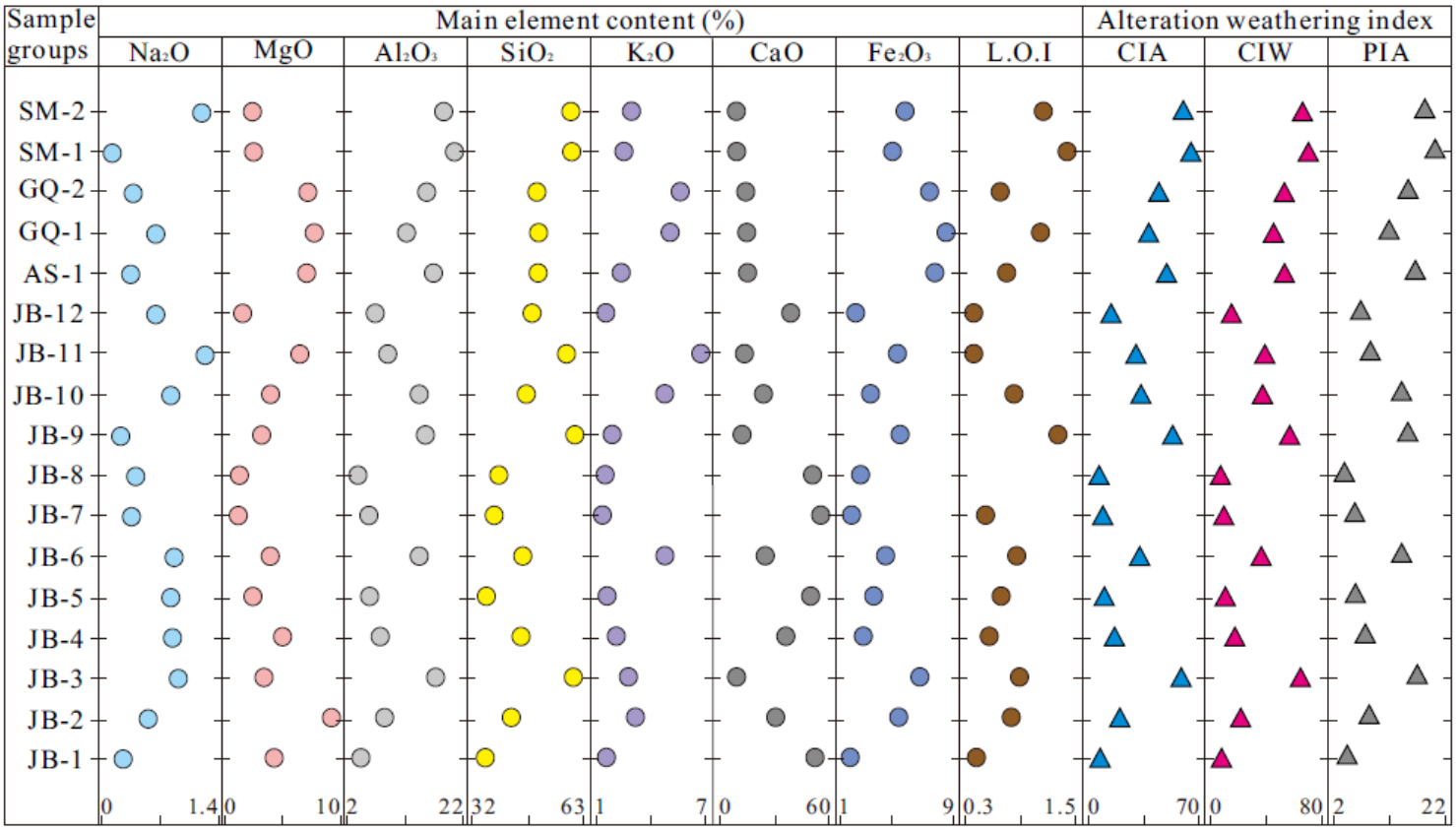

Figure 4

Main element contents and alteration weathering index of the PWR.

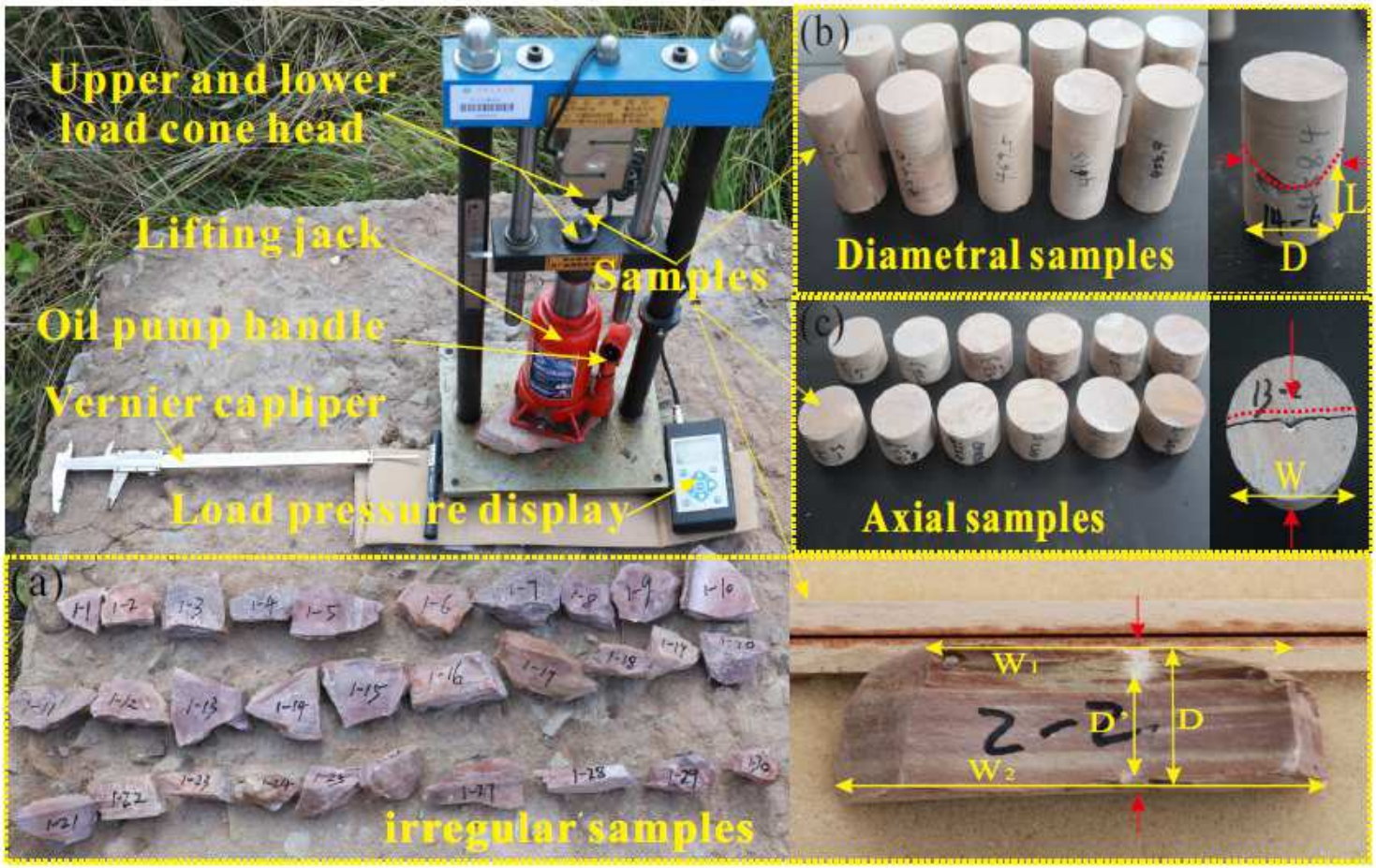

Figure 5

Point load instrument (YXDZ-10) and the definitions of L, D, D', W1 and W2.

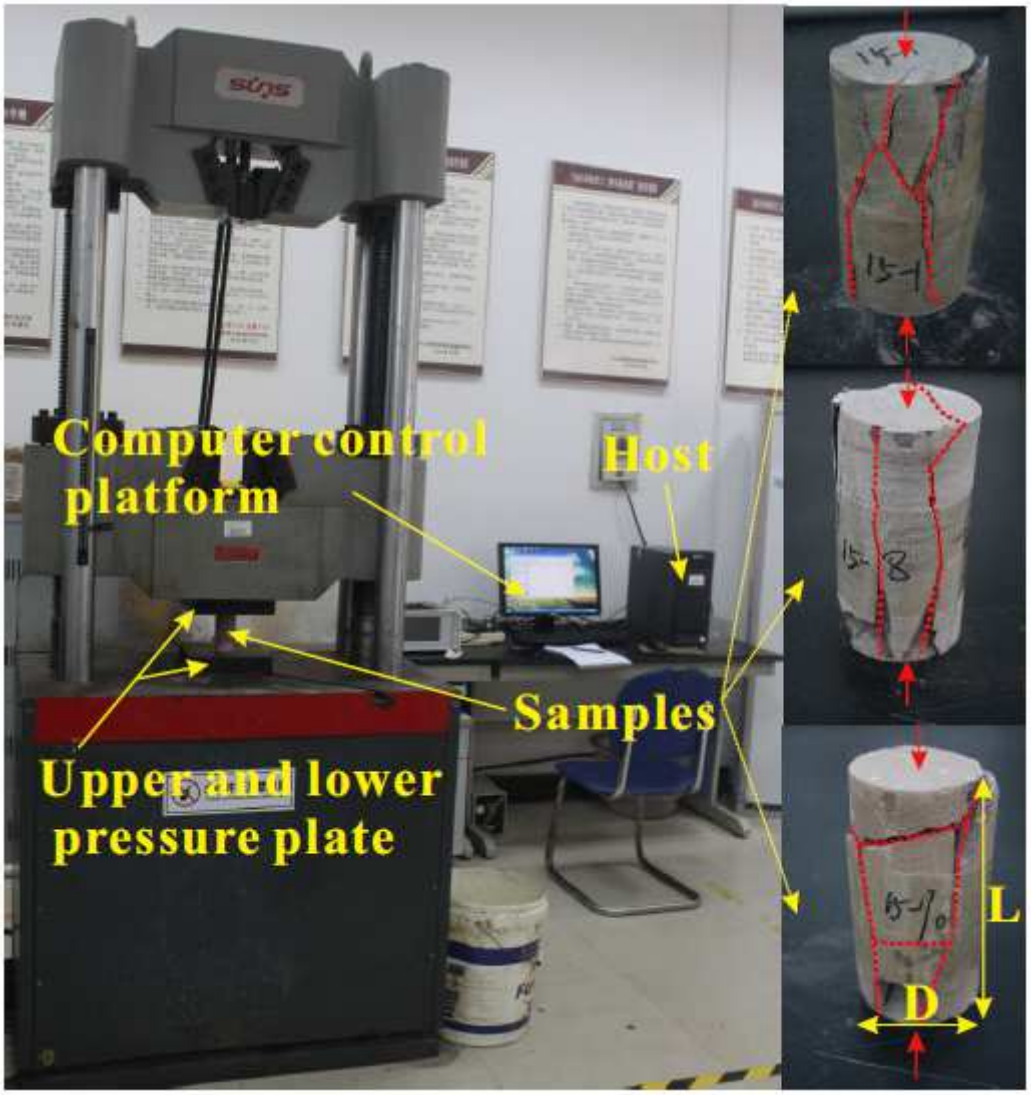

Figure 6

D-1000 electro-hydraulic servo universal testing machine.

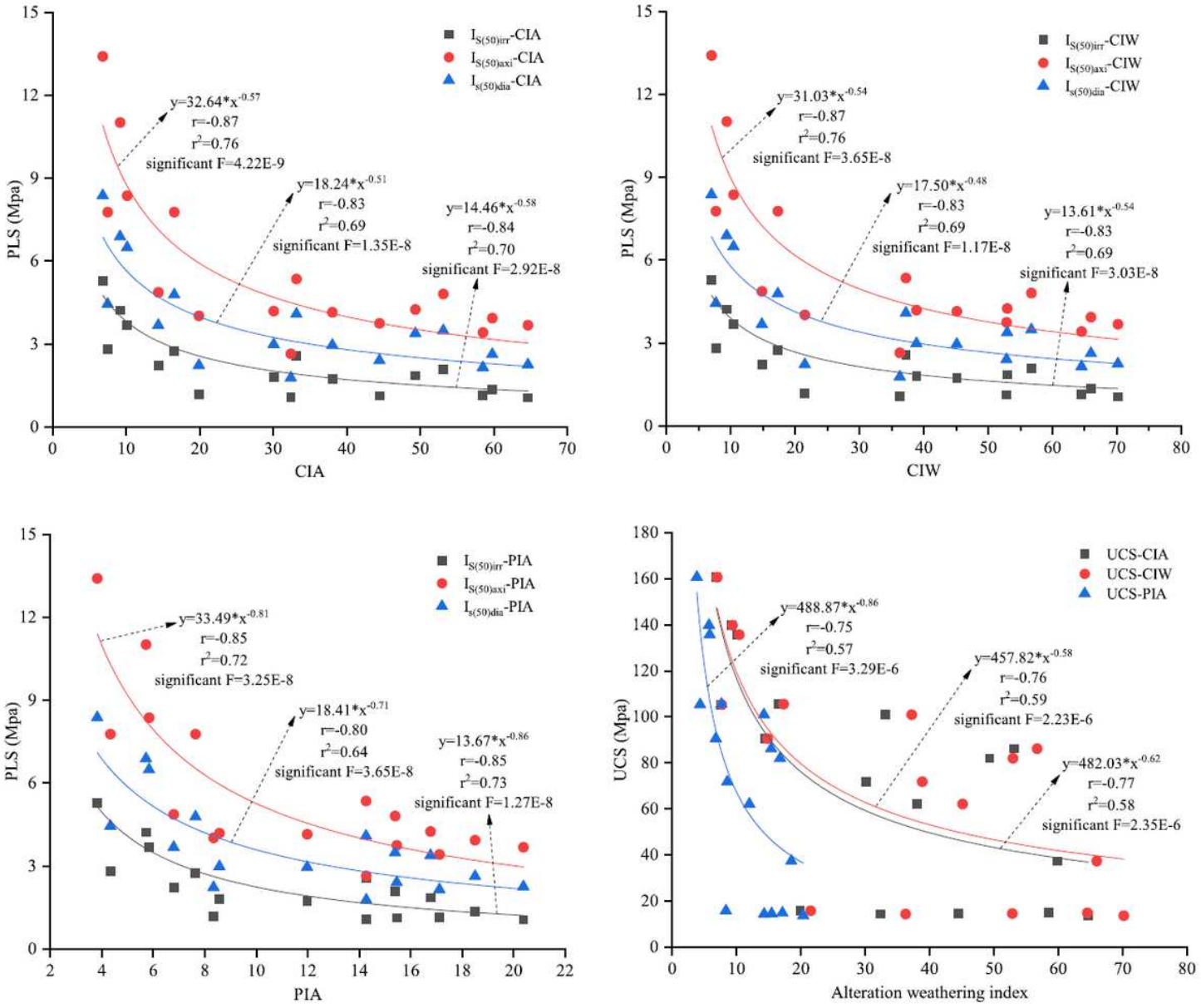

Figure 7

Relationships between strength of PWR and CIA, CIW, and PIA.

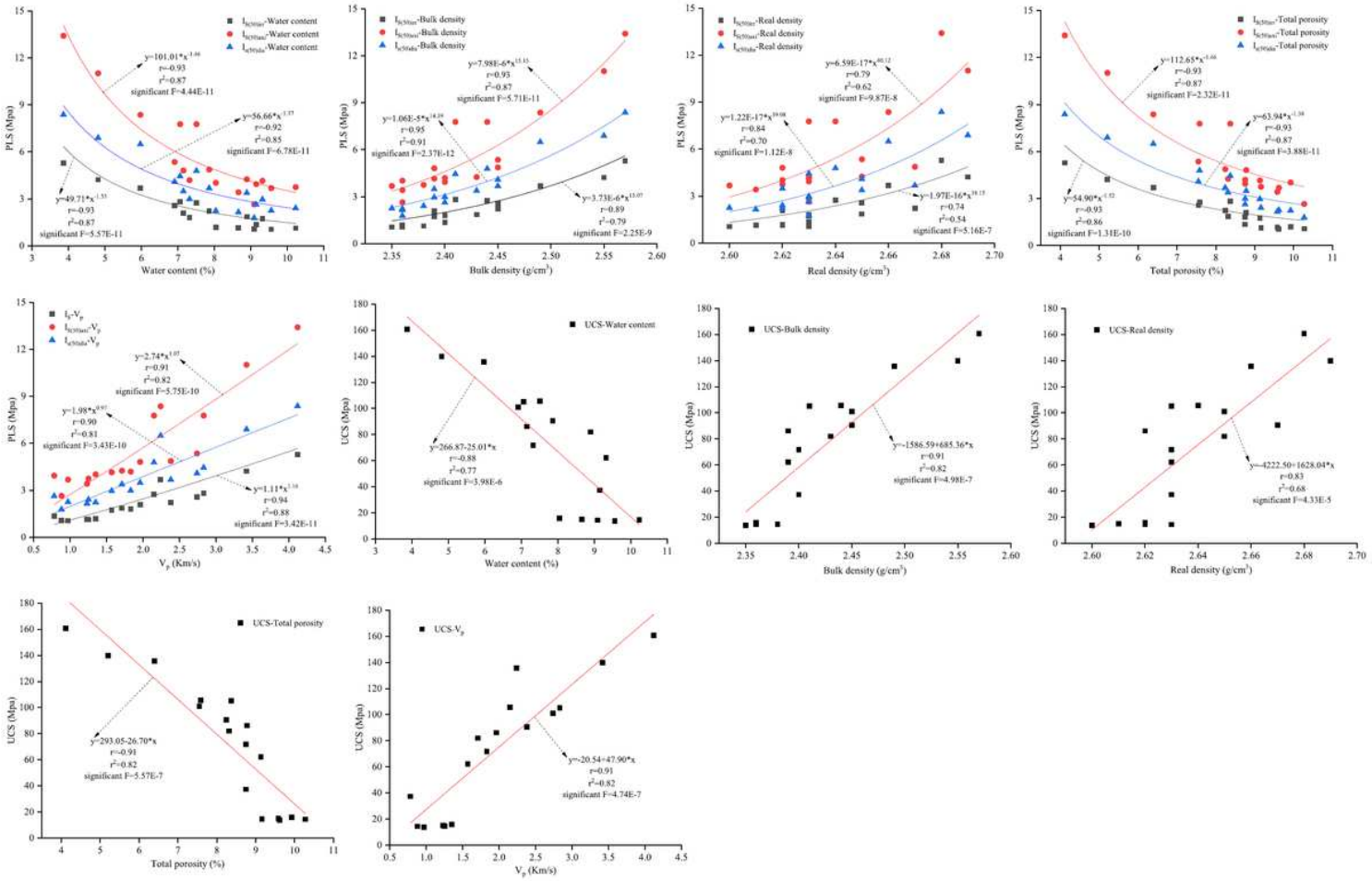

Figure 8

Relationships between strength of PWR and physical properties.

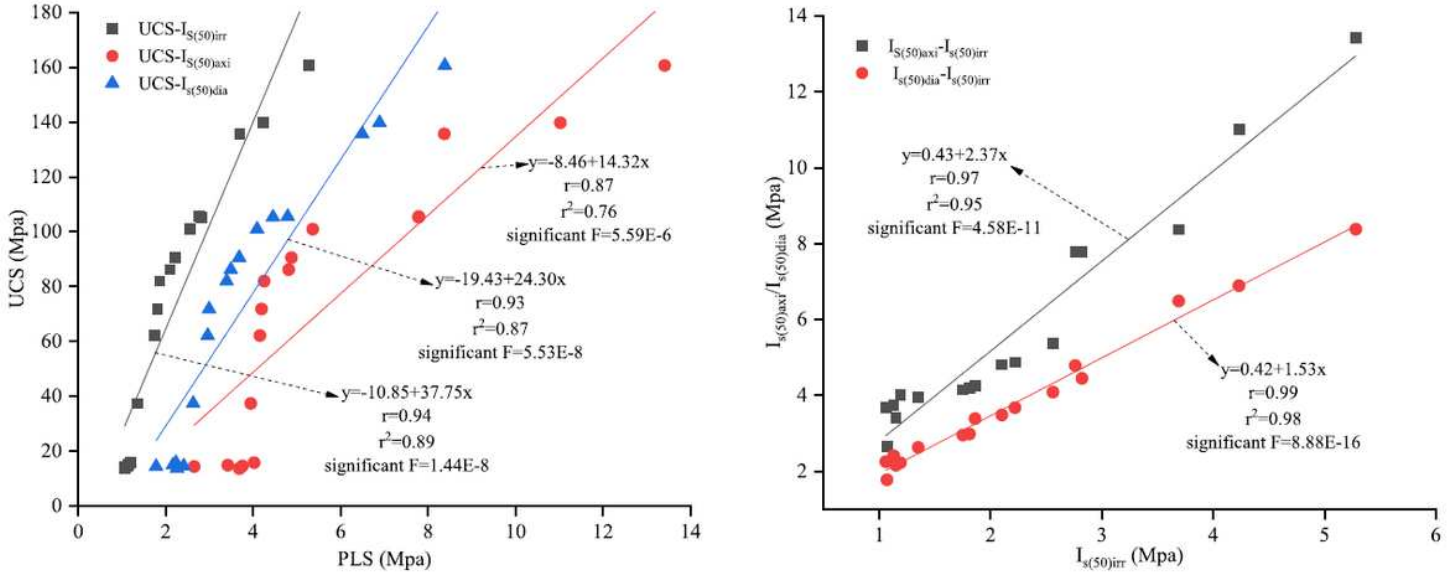

Figure 9

Relationships between the UCS and PLS, axial PLS, diametral PLS and irregular PLS.